Journal of Magnetic Resonance **146,** 255–259 (2000)
doi:10.1006/jmre.2000.2157, available online at http://www.idealibrary.com on IDEAL®

Determination of Backbone Angle ψ in Proteins Using a TROSY-Based α/β-HN(CO)CA-J Experiment

Perttu Permi,*[,1] Ilkka Kilpeläinen,* and Arto Annila†

*Institute of Biotechnology, NMR Laboratory, P.O. Box 56, 00014 University of Helsinki, Finland; and
†VTT Biotechnology, FIN-02044 VTT, Espoo, Finland

Received April 7, 2000; revised June 15, 2000

Transverse relaxation-optimized NMR experiment (TROSY) for the measurement of three-bond scalar coupling constant between $^{1}H^{\alpha}_{i-1}$ and $^{15}N_i$ defining the dihedral angle ψ is described. The triple-spin-state-selective experiment allows measurement of $^{3}J_{H^{\alpha}N}$ from $^{13}C^{\alpha}$, ^{15}N, and $^{1}H^{N}$ correlation spectra H_2O with minimum resonance overlap. Transverse relaxation of $^{13}C^{\alpha}$ spin is minimized by using spin-state-selective filtering and by acquiring a signal longer in ^{15}N-dimension in a manner of semi-constant-time TROSY evolution. The $^{3}J_{H^{\alpha}N}$ values obtained with the proposed α/β-HN(CO)CA-J TROSY scheme are in good agreement with the values measured earlier from ubiquitin in D_2O using the HCACO[N] experiment. © 2000 Academic Press

Key Words: **coupling constants; semi-constant-time; spin-state-selective filters; TROSY; ubiquitin.**

INTRODUCTION

Protein main chain conformation is defined by two dihedrals, ϕ and ψ. These Ramachandran angles relate to three-bond J coupling constants via Karplus relations (*1, 2*). Six different three-bond scalar couplings, $^{3}J_{H^{N}H^{\alpha}}$, $^{3}J_{H^{N}C'}$, $^{3}J_{H^{N}C^{\beta}}$, $^{3}J_{C'H^{\alpha}}$, $^{3}J_{C'C'}$, and $^{3}J_{C'C^{\beta}}$ define dihedral ϕ, and there are several methods to measure these few hertz couplings (*3–9*). The ψ torsion is more difficult to determine from the three ^{3}J couplings, i.e., $^{3}J_{H^{\alpha}N}$, $^{3}J_{NC^{\beta}}$, and $^{3}J_{NN}$ (*10–12*). The latter two couplings are always very small ($^{3}J_{NC^{\beta}} < 0.4$ Hz, $^{3}J_{NN} < 0.35$ Hz). Therefore their applicability for the determination of ψ is somewhat limited (*12, 13*). However, for perdeuterated samples these two couplings are the only ones available. It is also possible to extract information on ψ directly from dipole–dipole ^{15}N–$^{1}H^{N}$ and $^{13}C^{\alpha}$–$^{1}H^{\alpha}$ or dipole $^{13}C^{\alpha}$–$^{1}H^{\alpha}$ and $^{13}C'$ chemical shift anisotropy (CSA) cross-correlated relaxation rates (*14, 15*) provided that the molecular rotational correlation time, τ_c, is known.

In this paper we focus on measurement of three-bond scalar coupling between $^{15}N_i$ and $^{1}H^{\alpha}_{i-1}$, which has the largest dependence on dihedral angle ψ among the three ^{3}J couplings. The early theoretical calculations predicted values for $^{3}J_{H^{\alpha}N}$ from -6.6 to $+1.1$ Hz. It was shown, however, that this parametrization provides poor results (*11, 16*). Wang and Bax recorded from protein ubiquitin $^{3}J_{H^{\alpha}N}$ data ranging from 0.1 to -1.9 Hz for reparametrization of the Karplus curve (*11*). There are not, to the best of our knowledge, many experimental schemes for measurement of this inherently relatively small scalar coupling. The $^{3}J_{H^{\alpha}N}$ has been measured previously using an E.COSY-type HCA-CO[N] correlation experiment, using ^{15}N as a passive spin during t_1 and t_3 periods (*11*). Although it is possible to record the HCACO spectrum in H_2O, the residual water signal often distorts the adjacent $^{1}H^{\alpha}$ signals, hindering data analysis. The dissolvation of a protein sample into D_2O is an additional task, and due to a viscosity of D_2O larger than that of H_2O, the protein's rotational correlation time is increased. An alternative approach is an HN(CO)CA E.COSY-type experiment (*10*), where $^{1}H^{\alpha}$ acts as a passive spin during t_1 and t_2 evolution periods. We base the measurement of $^{3}J_{H^{\alpha}N}$ on this kind of experiment, which opens the possibility of exploiting the most slowly relaxing ^{15}N–^{1}H multiplet component by a transverse relaxation-optimized (TROSY) selection (*17–19*). For precise measurement of $^{3}J_{H^{\alpha}N}$ we apply spin-state-selective filtering (*20, 21*) and use a semi-constant-time evolution (*22*) period for ^{15}N chemical shift and ^{15}N–$^{1}H^{\alpha}$ coupling during t_2. There are several advantages over the HCACO[N] experiment when using the proposed scheme. The gradient and sensitivity-enhanced TROSY implementation will yield a distortion-free ^{15}N, $^{1}H^{N}$ correlation spectrum not disturbed by the water resonance far away. The relaxation time for ^{15}N especially for the TROSY component is much more favorable than that of the $^{1}H^{\alpha}$ spin. We can alleviate the signal decay due to rapidly relaxing the $^{13}C^{\alpha}$ spin by separating partly overlapping $^{13}C^{\alpha}$–$^{1}H^{\alpha}$ doublet components into two subspectra by spin-state-selective filtering. In this way, the t_1 acquisition time can be kept short, and also unnecessary spectral crowding is removed. Finally, the semi-constant-time TROSY evolution period (*23, 24*) compensates for the short t_1 acquisition.

[1] To whom correspondence should be addressed. Fax: +358 9 191 59541. E-mail: Perttu.Permi@helsinki.fi.

1090-7807/00 $35.00

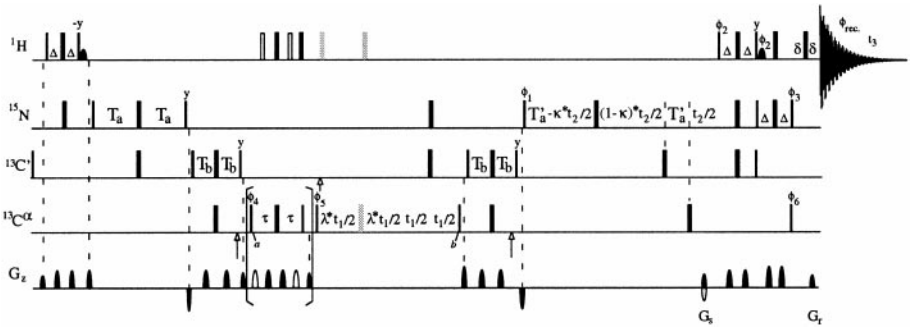

FIG. 1. Gradient-selected sensitivity-enhanced α/β-HN(CO)CA-J TROSY pulse sequence for determination of scalar couplings from 3D $^{13}C^{\alpha}$–^{15}N–$^{1}H^{N}$ correlation spectra. Narrow (wide) bars correspond to 90° (180°) pulses, with phase x unless otherwise indicated. Half-ellipses denote water-selective 90° pulses to obtain water-flip-back. All 90° (180°) pulses for $^{13}C'$ and $^{13}C^{\alpha}$ are applied with a strength of $\Omega/\sqrt{15}$ ($\Omega/\sqrt{3}$), where Ω is the frequency difference between the centers of the $^{13}C'$ and $^{13}C^{\alpha}$ regions. The ^{1}H, ^{15}N, $^{13}C'$, and $^{13}C^{\alpha}$ carrier positions are 4.7 (water), 120 (center of ^{15}N spectral region), 175 (center of $^{13}C'$ spectral region), and 55 ppm (center of $^{13}C^{\alpha}$ spectral region), respectively. Quadrature detection in the F_1 dimension is obtained by altering the phase of ϕ_5 according to States–TPPI (*33*). For quadrature detection and TROSY selection in F_2, two data sets, both for the in- and antiphase spectra, are collected: (I) $\phi_2 = x$, $\phi_3 = y$; (II) $\phi_2 = -x$, $\phi_3 = -y$, with simultaneous change in gradient polarity (*19*). The data processing is according to the sensitivity-enhanced method (*34*). The delays employed are $\Delta = 1/(4J_{NH})$; $T_a = 1/(4J_{NC'})$; $T'_a = T_a - \Delta$; $T_b = 1/(4J_{C'C\alpha})$; $\tau = 1/(4J_{CH})$; $\lambda \geq 0$; $0 \leq \kappa \leq (T_a - \Delta)/t_{2,max}$. Phase cycling for the in-phase spectrum is as follows: $\phi_1 = x$; $\phi_4 = x, -x$; $\phi_5 = x$; $\phi_6 = 2(x), 2(-x)$; $\phi_{rec.} = x, -x$; for the antiphase spectrum: $\phi_4 = y, -y$. The arrows indicate the positions of the Bloch–Siegert compensation pulses. The resolution in the ^{15}N dimension is improved by implementing the ^{15}N chemical shift and the ^{15}N–$^{1}H^{\alpha}$ coupling evolution in a semi-constant-time manner. If accordion style spectroscopy for J multiplication in t_1 is not used, the 180° pulses denoted by gray rectangles should be omitted. Pulsed field gradients are inserted as indicated for coherence transfer pathway selection and residual water suppression. For each scheme, the in- and antiphase data are recorded in an interleaved manner and subsequently added and subtracted to separate the multiplet components into two subspectra. Gradient strengths (durations) are optimized for the highest sensitivity: $G_s = 30$ G/cm (1.25 ms), $G_r = 29.6$ G/cm (0.125 ms).

RESULTS AND DISCUSSION

We now describe a three-dimensional TROSY-based spin-state-selective α/β-HN(CO)CA-J experiment for the measurement of $^{3}J_{H\alpha N}$ coupling in protonated samples (Fig. 1). The gradient-selected sensitivity-enhanced TROSY scheme, spin-state-selective filtering, and a semi-constant-time evolution of ^{15}N are implemented to the HN(CO)CA E.COSY experiment (*10*). The flow of coherence is

$$^{1}H^{N} \xrightarrow{J_{NH}} {}^{15}N \xrightarrow{J_{NC'}} {}^{13}C' \xrightarrow{J_{C'C^{\alpha}}} {}^{13}C^{\alpha} \xrightarrow{J_{CH}} {}^{13}C^{\alpha}(t_1) \xrightarrow{J_{C'C^{\alpha}}} {}^{13}C' \xrightarrow{J_{NC'}} {}^{15}N(t_2) \xrightarrow{J_{NH}} {}^{1}H^{N}(t_3),$$

where t_1, t_2, and t_3 are the evolution and acquisition times, respectively. Couplings used for magnetization transfer are indicated above the arrows. The spin-state-selective α/β-half-filter element is placed prior to the t_1 evolution period for the purpose of subspectral editing.

In this approach we first transfer the $^{1}H^{N}$ magnetization to the $^{13}C^{\alpha}_{i-1}$ spin via $^{15}N_i$ and $^{13}C'_{i-1}$ spins utilizing standard building blocks for coherence transfer. The desired magnetization can be denoted by the density operator $8H^{N}_{z}N_{z}C'_{z}C^{\alpha}_{y}$ at time point a. At this point, by inserting a spin-state-selective filter element into the pulse sequence, we can edit the $^{13}C^{\alpha}_{i-1}$ magnetization with respect to its directly bound $^{1}H^{\alpha}$ spin. In the first experiment, referred to as the in-phase experiment, two 180° (^{1}H) pulses marked with unfilled bars are applied at the midpoint of delays τ. The desired magnetization is transferred to $8H^{N}_{y}N_{z}C'_{z}C^{\alpha}_{z}$ coherence before the ensuing gradient pulse, which serves to purge undesired magnetization components in a way analogous to pulsed-field gradient z filtering (PFG-z-filter) (*vide infra*). The coupling between the $^{13}C^{\alpha}$ and $^{1}H^{\alpha}$ spins emerges during the subsequent t_1 evolution period when the $^{13}C^{\alpha}$ chemical shift is labeled. In order to reduce experimental time, accordion style spectroscopy (*25*) can be utilized in the F_1 dimension; i.e., $^{1}J_{C^{\alpha}H^{\alpha}}$ can be scaled up by λ if simultaneous 180° pulses are applied to the proton and C^{α} as shown in Fig. 1. Thus, the desired magnetization is in the form of

$$H^{N}_{z}N_{z}C'_{z}C^{\alpha}_{y}\cos(\omega_{C^{\alpha}}t_1)\cos(\pi\,{}^{1}J_{C^{\alpha}H^{\alpha}}(1+\lambda)t_1)\cos(\pi\,{}^{1}J_{C^{\alpha}C^{\beta}} \times (1+\lambda)t_1) + H^{N}_{z}N_{z}C'_{z}C^{\alpha}_{y}H^{\alpha}_{z}\sin(\omega_{C^{\alpha}}t_1)\sin(\pi\,{}^{1}J_{C^{\alpha}H^{\alpha}} \times (1+\lambda)t_1)\cos(\pi\,{}^{1}J_{C^{\alpha}C^{\beta}}(1+\lambda)t_1)$$

for the in-phase experiment at the end of the t_1 evolution period (time point b). Subsequently, the magnetization is transferred back to ^{15}N and its chemical shift evolution is monitored during the t_2 evolution implemented into the $^{13}C'$–^{15}N back-transfer step in a semi-constant time manner.

In the second experiment, referred to as the antiphase ex-

periment, two 180° (^{1}H) pulses marked with filled bars are applied immediately before 180° ($^{13}C^{\alpha}$) and 90° ($^{13}C^{\alpha}$) pulses, respectively. In addition, the phase of the $90^{\circ}_{\phi 4}$ ($^{13}C^{\alpha}$) pulse is shifted 90° with respect to the in-phase experiment. Thus, the desired magnetization is in the form of $16H_z^N N_z C'_z C_z^{\alpha} H_z^{\alpha}$ coherence before the ensuing gradient pulse, which will purge dispersive components of magnetization arising from J mismatch. Consequently, the desired magnetization at time point b is in the form of

$$H_z^N N_z C'_z C_y^{\alpha} \sin(\omega_{C^{\alpha}} t_1) \sin(\pi\, {}^1J_{C^{\alpha}H^{\alpha}}(1+\lambda)t_1) \cos(\pi\, {}^1J_{C^{\alpha}C^{\beta}} \times (1+\lambda)t_1) + H_z^N N_z C'_z C_y^{\alpha} H_z^{\alpha} \cos(\omega_{C^{\alpha}} t_1) \cos(\pi\, {}^1J_{C^{\alpha}H^{\alpha}} \times (1+\lambda)t_1) \cos(\pi\, {}^1J_{C^{\alpha}C^{\beta}}(1+\lambda)t_1)$$

in the antiphase experiment, and is subsequently transferred back to the amide proton analogously to the in-phase experiment.

As we allow the evolution of $^1J_{HNN}$ and $^3J_{H^{\alpha}N}$ to take place during t_2, we can select the most slowly relaxing ^{15}N–^{1}H^N cross peak by the gradient-selected sensitivity-enhanced TROSY scheme (*19*), and create a familiar E.COSY pattern (*26*), revealing the small $^3J_{H^{\alpha}N}$ coupling. In order to obtain sufficient resolution in the F_2 dimension, the ^{15}N chemical shift evolution is implemented as a semi-constant-time TROSY evolution (*23, 24*). It is advantageous to concatenate the $^{13}C'$–^{15}N back-INEPT and the first α/β filter in the generalized TROSY scheme (*24, 27*) to minimize signal loss due to ^{15}N transverse relaxation. The last two 90° pulses on carbon serve as purge pulses for the undesired magnetization components arising, e.g., from the J mismatch of ^{15}N–$^{13}C'$ coupling (*23*). Finally, post-acquisitional addition and subtraction of the in-phase and antiphase experiments will yield two 3D subspectra with correlations at $\omega_{C^{\alpha}}(i-1) + (1+\lambda)\pi^1 J_{C^{\alpha}H^{\alpha}}$, $\omega_N(i) - \pi^1 J_{NH} + \pi^3 J_{H^{\alpha}N}$, $\omega_{H^N}(i) + \pi^1 J_{NH}$ and $\omega_{C^{\alpha}}(i-1) - (1+\lambda)\pi^1 J_{C^{\alpha}H^{\alpha}}$, $\omega_N(i) - \pi^1 J_{NH} - \pi^3 J_{H^{\alpha}N}$, $\omega_{H^N}(i) + \pi^1 J_{NH}$, respectively. Clearly, this results in a correlation map with $^{13}C^{\alpha}_{i-1}$, $^{15}N_i$, $^1H_i^N$ at F_1, F_2, F_3, respectively, and $^3J_{H^{\alpha}N}$ is measured from the cross-peak displacement in the F_2 dimension. It should be noted that there is not enough resolution in the F_1 dimension to resolve $^1J_{C^{\alpha}C^{\beta}}$. In addition to $^3J_{H^{\alpha}N}$, we can measure $^1J_{C^{\alpha}H^{\alpha}}$ from the F_1 dimension. Interestingly, $^1J_{C^{\alpha}H^{\alpha}}$ shows also a large dependence on ψ, and thus it can be used at least as a qualitative probe for secondary structure (*28*). The data from $^3J_{H^{\alpha}N}$ and $^1J_{C^{\alpha}H^{\alpha}}$ available from the same experiment can conceivably be used simultaneously to determine the ψ angle.

There are few additional points to consider in achieving the optimal performance. Generally, TROSY is active during the ^{15}N–$^{13}C'$ out- and back-INEPT steps. It should be noted that two 180° (^{1}H) pulses during the in- and antiphase filter elements are applied to obtain optimal sensitivity. If only a single 180° (^{1}H) pulse was employed, this would interchange amide proton spin states for the ^{15}N–$^{13}C'$ out- and back-transfer steps, thus averaging relaxation rates for the fast and slowly relaxing multiplet components. However, by inserting another 180° (^{1}H) pulse during the filter elements, without perturbing $^1J_{CH}$ modulation or decoupling during the filtering, it is possible to maintain the TROSY effect during most of the pulse sequence. Likewise, if the J-multiplication approach is used during the t_1 period (by employing simultaneous 180° pulses on $^{13}C^{\alpha}$ and ^{1}H denoted by gray rectangles), it is necessary to apply an additional 180° (^{1}H) pulse prior to t_1 to preserve the TROSY effect during the latter part of the pulse sequence. Evidently, if neither spin-state-selective filtering nor the J-multiplication scheme is used, all 180° (^{1}H) pulses between the first ^{1}H–^{15}N INEPT and TROSY element should be omitted.

It is noteworthy that by using the semi-constant-time TROSY implementation, the 180° pulse for selective inversion of $^1H^N$ is no longer needed (*10*). In some unfortunate cases, where $^1H^N$ and $^1H^{\alpha}$ spins happen to resonate close to each other, the semi-selective inversion of $^1H^N$ might have some influence on the spin state of $^1H^{\alpha}$, resulting in a partial collapse of the desired E.COSY pattern.

The spin-state-selective filters are prone to a J crosstalk when coupling evolution does not exactly match the filter period. The J crosstalk is deleterious for subspectral editing; that is, in addition to the desired multiplet component, the minor component from the other spin state will be present in the subspectra. The intensity ratio of the principle component I_p to the minor component I_m in this case is

$$\frac{1+\sin\left(\pi\,\frac{J}{(2J_0)}\right)}{1-\sin\left(\pi\,\frac{J}{(2J_0)}\right)} = \frac{I_p}{I_m},$$

where J is the true coupling constant and the filter is matched to J_0. Owing to relatively uniform $^1J_{C^{\alpha}H^{\alpha}}$ values (140–150 Hz), excellent filtering is expected with respect to the J mismatch. The minor component arising from the J mismatch of the filter is over 30 times smaller than the major component in the range 120–170 Hz when $J_0 = 145$ Hz. Effects of J crosstalk on coupling constant measurements has been discussed earlier (*29–31*). In any case, if J crosstalk appears, the minor component can almost entirely be removed by taking an appropriate linear combination of the in- and antiphase spectra (*23, 32*).

The spin-state-selective filter elements are designed to suppress cross correlation between the CSA of $^{13}C^{\alpha}$ and the dipolar relaxation (DD) of $^{13}C^{\alpha}$–$^1H^{\alpha}$ by averaging relaxation rates of doublet components by the inversion of $^1H^{\alpha}$'s spin state during the filter elements, although $^{13}C^{\alpha}$ CSA is quite small.

Obviously, $^{13}C^{\alpha}_{i-1}$ couples also to H^N_{i-1} and H^N_i spins during the antiphase spin-state-selective filter element and the t_1 evolution period. These couplings are however very small compared to $^1J_{C^{\alpha}H^{\alpha}}$, i.e., 2 and 0.5 Hz, respectively, and their influence on filtering quality and lineshape is negligible. This holds true also for $^1J_{C^{\alpha}C^{\beta}}$.

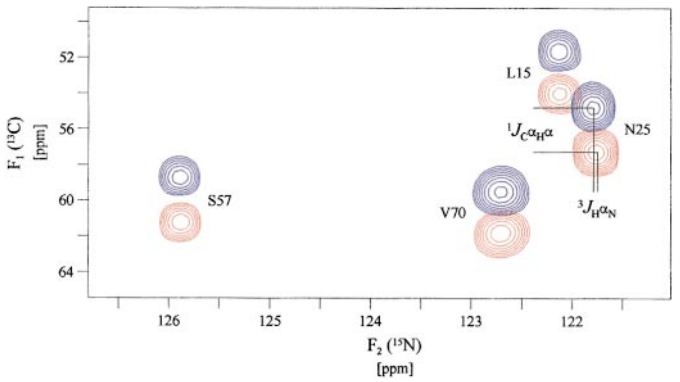

FIG. 2. F_1–F_2 expansion of the α/β-HN(CO)CA-*J* TROSY spectrum, recorded from 1.0 mM U-(^{15}N, ^{13}C) ubiquitin, 90%/10% H_2O/D_2O, 30°C at 500 MHz ^{1}H frequency, $t_{1,max}$, $t_{2,max}$ (t_3) = 3.15, 50.6 (64) ms. The $^1J_{C\alpha H\alpha}$ was multiplied by factor 2 with respect to $\omega_{C\alpha}$, i.e., $\lambda = 1$. Data were zero-filled to 1024 × 1024 × 512 data matrices and apodized with shifted squared sine-bell functions in all three dimensions. Up- (blue) and downfield (red) multiplet components, processed into separate subspectra, are shown superimposed for L15, D25, S57, and V70, taken at the $^1H^N$ (F_3) chemical shift of V26.

The t_1 evolution should be kept short because of rapid relaxation of $^{13}C^\alpha$ in larger proteins (~20 ms) and $^1J_{C^\alpha C^\beta}$ modulation. Consequently, the resolution in F_1 is limited. However, the spin-state-selective editing circumvents problems associated with the short acquisition time in F_1 by reducing spectral crowding and removing overlapping doublet components for a precise determination of $^1J_{C\alpha H\alpha}$. Obviously, in the case of determination of $^3J_{H\alpha N}$ only, t_1 can be extended by linear prediction to improve resolution.

The final point of interest concerns the semi-constant-time TROSY evolution period, which provides an improved resolution in the ^{15}N dimension. It is advantageous to follow the slowly relaxing TROSY component longer in the ^{15}N dimension to compensate for the modest resolution in the $^{13}C^\alpha$ dimension. It is worth mentioning that the experiment could also be recorded as a two-dimensional ^{15}N, $^1H^N$ TROSY correlation spectrum by omitting the $^{13}C^\alpha$ chemical shift and $^1J_{C\alpha H\alpha}$ coupling evolution period. In that case, the magnetization is in the form of $4H_z^N N_z C_z'$ and $8H_z^N N_z C_z' H_z^\alpha$ coherences prior to the ^{15}N chemical shift evolution in the in- and antiphase experiments, respectively. After ^{15}N chemical shift and ^{15}N–$^1H^\alpha$ coupling evolution, the signal of interest is in the form of $H_z^N N_y \cos(\omega_N t_1)\cos(\pi^3 J_{NH\alpha} t_1)$ and $H_z^N N_y \sin(\omega_N t_1)\sin(\pi^3 J_{NH\alpha} t_1)$ coherences in the in- and antiphase experiment, respectively, when omitting $^1J_{NH}$ evolution for simplicity. Thus, after the TROSY selection, correlations at $\omega_N(i) - \pi^1 J_{NH} + \pi^3 J_{H\alpha N}$, $\omega_{H^N}(i) + \pi^1 J_{NH}$ and $\omega_N(i) - \pi^1 J_{NH} - \pi^3 J_{H\alpha N}$, $\omega_{H^N}(i) + \pi^1 J_{NH}$ are available after appropriate addition and subtraction of the in- and antiphase spectra. The $^3J_{H\alpha N}$ coupling is measured from the cross-peak displacement in the ^{15}N dimension.

The proposed experiment for the measurement of the $^3J(^{15}N_i - {}^1H^\alpha_{i-1})$ scalar couplings was demonstrated with a 1.0 mM uniformly ^{15}N/^{13}C-enriched human ubiquitin, dissolved in 90%/10% H_2O/D_2O in a Wilmad 535PP NMR tube, pH 5.8, 50 mM sodium phosphate buffer, 30°C. Spectra were recorded on a Varian Unity Inova 500 NMR spectrometer, equipped with a triple-resonance probehead and an actively shielded *z*-axis gradient system. Figure 2 shows a representative portion of the overlaid F_1–F_2 plane of cross peaks taken from the $^1H^N$ chemical shift of V26. The subspectra were obtained by adding and subtracting cosine- and sine-modulated data sets, acquired with the pulse scheme shown in Fig. 1 in an interleaved manner. The vertical displacement of cross peaks yields $^1J_{C\alpha H\alpha}$, whereas the horizontal displacement yields $^3J_{H\alpha N}$. It was possible to measure 65 $^3J_{H\alpha N}$ couplings, i.e., excluding 6 glycines and 3 residues preceding prolines, from a 3D spectra collected in 46 h. Additionally, cross peaks for D52 and I23 were not observed.

All the measured couplings fall in the range 0 to −1.85 Hz. The helical regions of ubiquitin, i.e., residues 24–34, show large $^3J_{H\alpha N}$ values between −1.2 and −1.85 Hz. Similar values were also found for a short α-helix extending from residue 56 to 59. The coupling constants were extracted simply from the 1D traces. More precise values could be obtained by taking into account the entire signal of a 2D cross peak. The measured $^3J_{H\alpha N}$ couplings were compared with the corresponding values determined by Wang and Bax using the HCACO[N] E.COSY-type experiment (*11*). Comparison of 63 $^3J_{H\alpha N}$ couplings gave a 0.17-Hz pairwise root-mean-square-deviation (RMSD) (Fig. 3). The parametrization of the Karplus curve by Wang and Bax (*11*) gives a residual RMSD of 0.16 Hz compared with 0.19 Hz obtained with our data. A reparametrization on the basis of our data would improve the fit only by 0.02 Hz, which is within the precision of our measurements. The data suggest that there is no systematic deviation between these two methods. However, $^1H^\alpha$ spin flip during the delay used for $^{13}C^\alpha$-to-$^{13}C'$ back transfer may lead to systematic errors in the case of a large

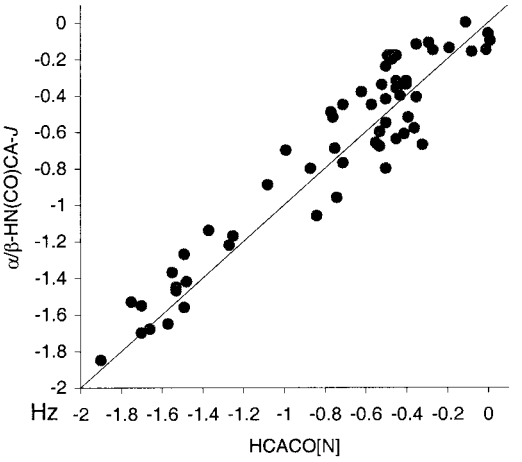

FIG. 3. Correlation of $^3J_{H\alpha N}$ coupling constants measured from spectra acquired with the α/β-HN(CO)CA *J* TROSY vs values measured by Wang and Bax from the HCACO[N] experiment (*11*). The pairwise root-mean-squared deviation is 0.17 Hz. The couplings were measured from separation of cross-peak placements in the F_1–F_2 plane between two subspectra.

protein because observed splittings have a bias toward smaller values. This problem can be alleviated by shortening the latter delay $2*T_b$. The HCACO[N] experiment uses ^{15}N, which has a long T_1, as a passive spin. However, the α/β-HN(CO)CA-J scheme provides a correlation map and relaxation properties of $^1H^N$ and ^{15}N spins more favorable than that of $^1H^\alpha$ and $^{13}C'$ spins used in the HCACO[N] experiment. Also the time for the rapidly relaxing $^{13}C^\alpha$ spin being in the transverse plane can be minized in the proposed scheme.

CONCLUSIONS

In summary, a transverse relaxation optimized α/β-HN-(CO)CA-J pulse sequence for the measurement of $^3J_{H\alpha N}$ couplings that define the backbone ψ torsion angle is described. The proposed method combines desired features of the semi-constant-time TROSY evolution, spin-state-selective filtering, and good resolution of 3D experiment to enable convenient and reliable measurement of $^3J_{H\alpha N}$ in proteins not requiring per-deuteration ($\sim$20–25 kDa). In addition to $^3J_{H\alpha N}$, the experiment yields $^1J_{C\alpha H\alpha}$ coupling and $^{13}C^\alpha$ chemical shift data, therefore providing a wealth of information to restrain ψ in structure calculations.

ACKNOWLEDGMENT

This work was supported by the Academy of Finland.

REFERENCES

1. M. Karplus, *J. Chem. Phys.* **30,** 11–15 (1959).
2. V. F. Bystrov, *Prog. NMR Spectrosc.* **10,** 44–81 (1976).
3. G. W. Vuister and A. Bax, *J. Am. Chem. Soc.* **115,** 7772–7777 (1993).
4. H. Aitio and P. Permi, *J. Magn. Reson.* **143,** 391–396 (2000).
5. R. Weisemann, H. Rüterjans, H. Schwalbe, J. Schleucher, W. Bermel, and C. Griesinger, *J. Biomol. NMR* **4,** 231–240 (1994).
6. J.-S. Hu and A. Bax, *J. Am. Chem. Soc.* **118,** 8170–8171 (1996).
7. S. J. Archer, M. Ikura, D. A. Torchia, and A. Bax, *J. Magn. Reson.* **95,** 636–641 (1991).
8. A. Rexroth, P. Schmidt, S. Szalma, T. Geppert, H. Schwalbe, and C. Griesinger, *J. Am. Chem. Soc.* **117,** 10,389–10,390 (1995).
9. A. Meissner, T. Schulte-Herbrüggen, and O. W. Sørensen, *J. Am. Chem. Soc.* **120,** 3803–3804 (1998).
10. S. Seip, J. Balbach, and H. Kessler, *J. Magn. Reson. B* **104,** 172–179 (1994).
11. A. C. Wang and A. Bax, *J. Am. Chem. Soc.* **117,** 1810–1813 (1995).
12. F. Löhr and H. Rüterjans, *J. Magn. Reson.* **132,** 130–137 (1998).
13. R. Konrat, D. R. Muhandiram, N. A. Farrow, and L. E. Kay, *J. Biomol. NMR* **9,** 409–422 (1997).
14. B. Reif, M. Hennig, and C. Griesinger, *Science* **276,** 1230–1233 (1997).
15. D. Yang, K. H. Gardner, and L. E. Kay, *J. Biomol. NMR* **11,** 213–220 (1998).
16. K. D. Kopple, A. Ashan, and M. Barfield, *Tetrahedron Lett.* **38,** 3519–3522 (1978).
17. K. Pervushin, R. Riek, G. Wider, and K. Wüthrich, *Proc. Natl. Acad. Sci. U.S.A.* **94,** 12,366–12,371 (1997).
18. P. Andersson, A. Annila, and G. Otting, *J. Magn. Reson.* **133,** 364–367 (1998).
19. J. Weigelt, *J. Am. Chem. Soc.* **120,** 10,778–10,779 (1998).
20. A. Meissner, J. Ø. Duus, and O. W. Sørensen, *J. Biomol. NMR* **10,** 89–94 (1997).
21. P. Andersson, J. Weigelt, and G. Otting, *J. Biomol. NMR* **12,** 435–441 (1998).
22. T. M. Logan, E. T. Olejniczak, R. X. Xu, and S. W. Fesik, *J. Biomol. NMR* **3,** 225–231 (1993).
23. P. Permi and A. Annila, *J. Biomol. NMR* **16,** 221–227 (2000).
24. P. Permi, P. R. Rosevear, and A. Annila, *J. Biomol. NMR* **17,** 43–54 (2000).
25. G. Bodenhausen and R. R. Ernst, *J. Magn. Reson.* **45,** 367–373 (1981).
26. C. Griesinger, O. W. Sørensen, and R. R. Ernst, *J. Am. Chem. Soc.* **107,** 6394–6936 (1985).
27. M. Salzmann, G. Wider, K. Pervushin, and K. Wüthrich, *J. Biomol. NMR* **15,** 181–184 (1999).
28. S. Grzesiek and A. Bax, *J. Biomol. NMR* **3,** 185–204 (1993).
29. A. Meissner, T. Schulte-Herbrüggen, and O. W. Sørensen, *J. Am. Chem. Soc.* **120,** 7989–7990 (1998).
30. P. Permi, S. Heikkinen, I. Kilpeläinen, and A. Annila, *J. Magn. Reson.* **140,** 32–40 (1999).
31. P. Permi, T. Sorsa, I. Kilpeläinen, and A. Annila, *J. Magn. Reson.* **141,** 44–51 (1999).
32. M. D. Sørensen, A. Meissner, and O. W. Sørensen, *J. Magn. Reson.* **137,** 237–242 (1999).
33. D. Marion, M. Ikura, R. Tschudin, and A. Bax, *J. Magn. Reson.* **85,** 393–399 (1989).
34. L. E. Kay, P. Keifer, and T. Saarinen, *J. Am. Chem. Soc.* **114,** 10,663–10,665 (1992).